Viscous drag of a solid sphere straddling a spherical or flat surface

Krassimir D. Danov[a)] and Rumiana Dimova
Laboratory of Thermodynamics and Physico-chemical Hydrodynamics, Faculty of Chemistry,
Sofia University, 1 J. Bouchier Ave., 1164 Sofia, Bulgaria

Bernard Pouligny
Centre de recherche Paul-Pascal, CNRS, Av. A. Schweitzer, 33600 Pessac, France

The aim of this paper is to compute the friction felt by a solid particle, of radius a, located across a flat or spherical interface of radius R, and moving parallel to the interface. This spherical interface can be a molecular film around an emulsion or aerosol droplet, the membrane of a vesicle or the soap film of a foam bubble. For simplicity, the acronym VDB is used to refer to either vesicle, drop, or bubble. The theory is designed as a tool to interpret surface viscosimetry experiments involving spherical probes attached to films or model membranes, taking care of the finite-size effects when the film encompasses a finite fluid volume. The surface of the VDB is a two-dimensional fluid, characterized by dilational (η_s^{dil}) and shear (η_s^{sh}) surface viscosities. The particle intercepts a circular disc in the interface, whose size depends on the particle penetration inside the VDB. The three-dimensional fluids inside and outside the interface may be different. The analysis holds in the low Reynolds number and low capillary number regime. A toroidal (x_1, x_2, ϕ) coordinate system is introduced, which considerably simplifies the geometry of the problem. Then the hydrodynamic equations and boundary conditions are written in x_1, x_2, ϕ. The solution is searched for the first-order Fourier component of the velocity field in the radial angle ϕ. Reformulating the equations in "two-vorticity-one-velocity" representation, one basically ends up with a set of equations in x_1, x_2 only. This set is numerically solved by means of the Alternating-Direction-Implicit method. Numerical results show that the particle friction is influenced both by the viscosity and by the finiteness of the VDB volume. Finite-size effects have two origins: a recirculation effect when a/R is not very small, and an overall rotation of the VDB-particle complex when η_s is very large. In principle, the theory allows for a quantitative determination of η_s whatever a/R, including the limit $a/R=0$ (flat interface). © *2000 American Institute of Physics.* [S1070-6631(00)01210-1]

I. INTRODUCTION

The problem of the motion of a solid particle along an interface separating two fluid phases has implications in technological and biological problems: for instance, emulsions can be stabilized by solid particles at the oil/water interface (Pickering emulsions[1]); the mobility of macroscopic inclusions or of organelles in contact with or across cell membranes also relates to the hydrodynamic problem discussed hereafter. A theory on the motion of a disc along a viscous interface/membrane was set up by Saffman[2,3] and later developed by Hughes *et al.*[4] In their approach the disc has the same thickness as the membrane, which is modeled as a two-dimensional viscous fluid. The Saffman–Hughes theory was successfully used to interpret experiments on Brownian motion of disc-like domains in a layer of fluid lipid,[5] and of proteins in membranes.[6,7] The disc problem was the matter of subsequent refinements, to include the effect of a wall parallel to the membrane (see the recent complete theory by Stone and Ajdari[8] and references therein).

The disc theory is not directly applicable to experiments with macroscopic three-dimensional probes, for instance spherical micron-sized particles on surfactant monolayers[9,10] at the water/air interface. This kind of system was theoretically addressed by Danov *et al.*[11] Their approach took into account both the interfacial viscous properties and the hydrodynamic contribution of the part of the floating particle protruding in the water subphase. However, this approach was valid only for the air/liquid interface and a limited interval of three-phase contact angles at the particle surface. Danov *et al.*'s theory was worked out for particles which were predominantly immersed in the water phase, i.e., the contact angle θ (defined in the liquid phase), had to be less than about 100°. Recently, experiments[12] were carried out with latex microspheres attached to lipid membranes. In this situation, both sides of the film are made of a viscous fluid, and then both sides of the particle contribute to the friction. The interpretation of the experimental results in Ref. 12 was based on regarding the studied system as a superposition of two "air/water" systems with complementary contact angles, θ and $180° - \theta$. However, because of the above-mentioned restriction, the superposition approach is inapplicable for spheres with contact angles far from 90°. Moreover, Danov *et al.*'s theory[11] was elaborated only for flat and infinite interfaces. As the particle in the experiments in Ref.

[a)] Author to whom correspondence should be addressed; electronic mail: KRASSIMIR.DANOV@LTPH.BOL.BG
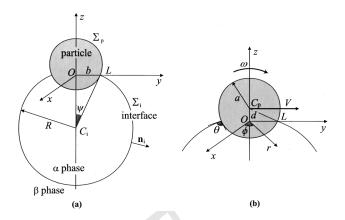
FIG. 1. (a) The problem: a particle of radius a across a spherical interface of radius R separating two fluid phases, α and β; (b) detail of the VBD-particle complex; see text for symbol definitions.

12 is moving along a closed spherical membrane, i.e., a vesicle, the theoretical approach needs to account for the contribution of the finite water volume encompassed inside the vesicle.

Addressing this general problem is the purpose of this paper. Our goal is to compute the friction felt by a spherical solid particle straddling the interface of a spherical vesicle, droplet, or bubble (VDB) or flat interface. The interface is supposed to be a two-dimensional viscous fluid, characterized by dilation and shear surface viscosities.

In the following section, we start with the basic hydrodynamic equations and boundary conditions of the problem. We then introduce a toroidal coordinate system, (x_1, x_2, ϕ), whose axis contains the particle and the VDB centers. ϕ is the polar angle around this axis [see Fig. 1(b)]. Hydrodynamic equations are written in x_1, x_2, ϕ variables and the solution is searched for the first-order Fourier component in ϕ of the velocity and pressure fields. Reformulating the problem in the two-vorticity-one-velocity formalism allows us to transform the initial three-space-variable problem into a two-variable (x_1, x_2) one. The equations are solved numerically by means of the Alternating-Direction-Implicit method. Numerical results for the particle friction coefficient are given and commented on in Sec. III. There we identify the influences of the surface viscosity and of the finiteness of the VDB volume. As we will see, finite-size effects involve both a recirculation flow inside the VDB and an overall rotation of the VDB-particle complex when the interface is very viscous. A paragraph in Sec. III is dedicated to the limiting case of a flat infinite membrane. There we analyze the way in which the friction felt by the spherical particle depends on the contact angle, θ. This dependence is compared to that found in Saffman's theory for a disc. The results for the translational drag force are complemented by those for hydrodynamic torque acting on the particle, in the limit cases of an inviscid curved interface and of a viscous flat infinite one. Our main conclusions are summarized in Sec. IV.

II. MATHEMATICAL FORMULATION OF THE PROBLEM

A. Basic equations and boundary conditions

We consider the motion of a particle of radius a on a spherical viscous interface separating two fluid phases, see Fig. 1(a). The inner and external phases are denoted α and β, respectively. The interface is of finite radius, R, and meets the particle surface along a circular contact line indicated by L. In Fig. 1, ψ is the half angle of the cone defined by the VDB center and L (the limit $\psi = 0$ corresponds to a flat interface and will be commented on later). Σ_p and Σ_i refer to the particle surface and to the spherical interface correspondingly, while C_p and C_i indicate their centers. We denote by $Oxyz$ a system of Cartesian coordinates, whose origin is at the center of the particle contact line [see Fig. 1(b)]. The z-coordinate of the particle center is $d = \overline{OC_p}$. The particle moves parallel to the membrane, i.e., in the (Oy, Oz) plane with a translational velocity $\mathbf{V} = (0, V, 0)$ directed along the y-axis. We suppose that *the contact line does not move relatively to the surface of the particle*. This important assumption is suggested by the observations of Dietrich *et al.*[13] on polystyrene particles bound to lipid vesicles. These authors noticed that the contact angle would remain constant when the particle moved on the surface of the vesicle and that the membrane-particle contact line was ''pinned''[13] to the particle solid surface. The assumption of contact line pinning has the advantage of considerably simplifying the hydrodynamics of the problem. In particular, this eliminates the difficulties related to moving contact lines, such as the divergence of the shear rate or the multivaluedness of the flow field at the contact line.[14] In our description, the flow is everywhere single-valued and regular. Because of pinning of the contact line at the particle surface, rotations of the particle around Ox and Oy are forbidden. Rotation around Oz is forbidden by symmetry. The particle movement then reduces to a simple solid rotation around the VDB center. The corresponding angular velocity, ω, is given by

$$\omega = \frac{V \tan \psi}{b + d \tan \psi}, \tag{1}$$

where $b = \sqrt{a^2 - d^2}$ is the radius of the particle contact line, $b = \overline{OL}$ [see Fig. 1(a)]. The components of the velocity, $\mathbf{v}_p$, of an arbitrary point on the particle surface, Σ_p, in the cylindrical coordinate system, $Or\phi z$ [see Fig. 1(b)], are

$$v_{p,r} = [V + \omega(z_p - d)] \sin \phi,$$
$$v_{p,\phi} = [V + \omega(z_p - d)] \cos \phi, \tag{2}$$
$$v_{p,z} = -\omega r_p \sin \phi,$$

where (r_p, ϕ, z_p) are the coordinates of the point on Σ_p.

The two bulk phases on both sides of the spherical interface are assumed to be viscous and incompressible. Reynolds numbers in our problem are on the order of 10^{-4} or less, which allows us to safely ignore inertial terms. Consequently the Stokes equations hold for the local fluid velocity and for the pressure distribution[15] on both sides of the interface,

$$\nabla \cdot \mathbf{v}_k = 0, \quad \nabla p_k = \eta_k \nabla \cdot \nabla \mathbf{v}_k, \quad k = \alpha, \beta, \tag{3}$$

where ∇ is the spatial gradient. The subscript k refers to either α or β three-dimensional (3D) fluid. $\mathbf{v}$ and p are the velocity and pressure fields, respectively, and η_k is a 3D fluid dynamical viscosity.

We impose a no-slip boundary condition at the solid particle surface Σ_p for both fluid phases,

$$\mathbf{v}_k = \mathbf{v}_p, \quad k = \alpha, \beta. \tag{4}$$

We will consider a system where the particle motion perturbs the interface surface only very weakly, i.e., we work in the regime of small capillary number. In this situation the capillary forces dominate over the dynamic pressure contribution term and the spherical surface may be regarded as unperturbed (see the Appendix for a more detailed discussion). The balance of the tangential velocity components in both phases at Σ_i and the condition for no mass transfer across Σ_i lead to

$$\mathbf{v}_k = \mathbf{u}, \quad k = \alpha, \beta, \tag{5}$$

where $\mathbf{u}$ is the velocity of the two-dimensional continuous phase. Equation (5) represents the so-called kinematic boundary condition. The tangential stresses at the interface, Σ_i, balance the pressure jump across the interface from one bulk phase to another. This results in the dynamic boundary condition[16]

$$(\nabla_s \cdot \mathbf{P}_i) \times \mathbf{n}_i = \mathbf{n}_i \cdot (\mathbf{P}_\alpha - \mathbf{P}_\beta) \times \mathbf{n}_i. \tag{6}$$

∇_s is the surface gradient operator, $\mathbf{P}_i$ is the two-dimensional (2D) stress tensor at Σ_i, $\mathbf{n}_i$ is the unit normal to the interface oriented toward the continuous phase β, see Fig. 1(a), and $\mathbf{P}_\alpha$ and $\mathbf{P}_\beta$ are the bulk stress tensors in the enclosed and the external phases, respectively. For Newtonian fluids the latter are defined as[15]

$$\mathbf{P}_k = -p_k \mathbf{I} + \eta_k [\nabla \mathbf{v}_k + (\nabla \mathbf{v}_k)^T], \quad k = \alpha, \beta, \tag{7}$$
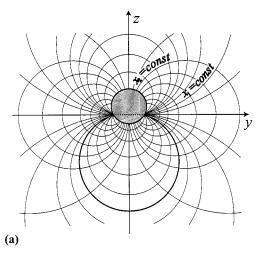
where $\mathbf{I}$ is the three-dimensional idemfactor and the superscript "T" denotes transposition. To define the interfacial stress tensor $\mathbf{P}_i$ introduced in Eq. (6), we adopt a simple linear Boussinesq–Scriven constitutive law[17,18]

$$\mathbf{P}_i = \sigma \mathbf{I}_s + (\eta_s^{\text{dil}} - \eta_s^{\text{sh}})(\mathbf{I}_s : \mathbf{D}_s)\mathbf{I}_s + 2\eta_s^{\text{sh}}\mathbf{D}_s, \tag{8a}$$

$$\mathbf{D}_s = \tfrac{1}{2}[(\nabla_s \mathbf{u}) \cdot \mathbf{I}_s + \mathbf{I}_s \cdot (\nabla_s \mathbf{u})^T]. \tag{8b}$$

In Eqs. (8a) and (8b), $\mathbf{I}_s$ is the 2d idemfactor and $\mathbf{D}_s$ is the interfacial rate-of-strain tensor. The physical parameters characterizing the surface Σ_i are the thermodynamical interfacial tension, σ, and the intrinsic shear and dilational membrane viscosities, η_s^{sh} and η_s^{dil}, respectively. Both viscosities are assumed constant. Note that surface viscosities have the dimension of a volume viscosity multiplied by a length. Here we follow the notation chosen, for instance, by Edwards et al.[16] In Saffman's and related theories,[2–4,8] the membrane shear viscosity is denoted $\eta_m h$ where h is the membrane thickness. With this notation, the membrane property, η_m, obviously has the dimension of a 3d fluid viscosity.

Due to the symmetry of the system under consideration, the velocity field satisfies the following condition along the $r = 0$ axis:
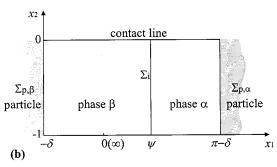

(a)

(b)

FIG. 2. (a) Toroidal mapping in the (y, z) plane; (b) numerical domain in toroidal coordinates.

$$\frac{\partial v_{k,r}}{\partial r} = 0, \quad \frac{\partial v_{k,\phi}}{\partial r} = 0, \quad v_{k,z} = 0, \quad k = \alpha, \beta. \tag{9}$$

B. Toroidal coordinates

We consider a $\phi = \text{constant}$ plane and define new (x_1, x_2) coordinates through

$$x = r(x_1, x_2)\cos\phi, \quad y = r(x_1, x_2)\sin\phi, \quad z = z(x_1, x_2), \tag{10}$$

with

$$r = \frac{b(1 - x_2^2)}{1 + 2x_2 \cos x_1 + x_2^2}, \quad z = \frac{2b x_2 \sin x_1}{1 + 2x_2 \cos x_1 + x_2^2}. \tag{11}$$

Putting $x_1 = \text{constant}$ or $x_2 = \text{constant}$ defines two sets of circles,

$$r^2 + (z + b \cot x_1)^2 = \frac{b^2}{\sin^2 x_1}; \tag{12a}$$

$$\left(r - b\frac{1 + x_2^2}{1 - x_2^2}\right)^2 + z^2 = \frac{4b^2 x_2^2}{(1 - x_2^2)^2}. \tag{12b}$$

This mapping of the (r, z) plane is illustrated in Fig. 2(a). When $b \neq 0$ this representation maps the infinite (r, z) plane into a finite rectangular domain in the (x_1, x_2) space [see Fig. 2(b)]: $-\delta \leq x_1 \leq \pi - \delta$ and $-1 \leq x_2 \leq 0$. The left boundary of the domain, $x_1 = -\delta$, is the portion of the particle surface in contact with the β phase, while the right one, $x_1 = \pi - \delta$, is

the portion in contact with the α phase. The interface, Σ_i, is simply represented by $x_1 = \psi$. The upper boundary, $x_2 = 0$, is the three-phase contact line ($r = b$, $z = 0$), and the lower boundary, $x_2 = -1$, is the Oz axis. Note that infinity ($r \rightarrow \infty$, $z \rightarrow \pm \infty$) reduces to a single point $(0, -1)$ in the (x_1, x_2) domain. The expressions for the metric coefficients, h_1 and h_2, can be derived from the relation between the coordinates, see Eq. (11),

$$h_1 = -\frac{1}{2bx_2}(1 + 2x_2 \cos x_1 + x_2^2), \quad h_2 = -x_2 h_1. \quad (13)$$

C. Two-vorticity-one-velocity formalism

Solving the system of Eqs. (3) coupled with the set of boundary conditions (4)–(6),(9) is very difficult. Obstacles specific to the structure of the equations [problems essentially arise from the second-order derivatives in Eq. (6)] are discussed elsewhere.[19–21]

We now proceed to setting out the equations in a numerically tractable form. Our first step is to retain only the first-order Fourier mode of the velocity field as a function of ϕ,

$$\mathbf{v}_k = [\nu_{k,1}(x_1, x_2) \sin \phi; \nu_{k,2}(x_1, x_2) \sin \phi; \nu_{k,\phi}(x_1, x_2) \cos \phi],$$

$$k = \alpha, \beta. \quad (14)$$

The second index to the velocity refers to components along the x_1 and x_2 coordinates, and along the perpendicular to the (x_1, x_2) plane. Basically, this mode is filtered out as a consequence of the symmetry of the system geometry and of the boundary conditions for the flow field in (x_1, x_2) coordinates. A similar approach was applied prior to this work in related problems; see, for instance, the papers by Goldman[22] and O'Neil.[23]

We now introduce the vorticity vector, $\mathbf{w}$, as

$$\mathbf{w}_k = \tfrac{1}{2} \nabla \times \mathbf{v}_k, \quad k = \alpha, \beta. \quad (15)$$

Likewise, we retain only the first Fourier mode of $\mathbf{w}$,

$$\mathbf{w}_k = [w_{k,1}(x_1, x_2) \cos \phi; w_{k,2}(x_1, x_2) \cos \phi;$$

$$w_{k,\phi}(x_1, x_2) \sin \phi], \quad k = \alpha, \beta. \quad (16)$$

It is equivalent to formulate the hydrodynamic problem in terms of $\nu_{k,1}$, $\nu_{k,2}$, $\nu_{k,\phi}$ or in terms of $w_{k,1}$, $w_{k,2}$, $\nu_{k,\phi}$. The equivalence between both presentations is the consequence of the following property:

$$\nu_{k,1} = h_1 \frac{\partial}{\partial x_1}(r\nu_{k,\phi}) + 2rw_{k,2},$$

$$\nu_{k,2} = h_2 \frac{\partial}{\partial x_2}(r\nu_{k,\phi}) - 2rw_{k,1}, \quad k = \alpha, \beta. \quad (17)$$

The second representation, known as the ''two-vorticity-one-velocity'' formalism,[19–21] has the advantage of leading to a set of differential equations whose derivatives are taken only along x_1 and x_2. These two-variable equations are set out below.

Substituting Eq. (17) in the equation of continuity, $\nabla \cdot \mathbf{v}_k = 0$, transforms the latter into a second-order partial differential equation for the ϕ-component of the velocity,

$$\frac{\partial}{\partial x_1}\left[\frac{rh_1}{h_2}\frac{\partial}{\partial x_1}(r\nu_{k,\phi})\right] + \frac{\partial}{\partial x_2}\left[\frac{rh_2}{h_1}\frac{\partial}{\partial x_2}(r\nu_{k,\phi})\right] - \frac{\nu_{k,\phi}}{h_1 h_2}$$

$$= 2\frac{\partial}{\partial x_2}\left(\frac{r^2 w_{k,1}}{h_1}\right) - 2\frac{\partial}{\partial x_1}\left(\frac{r^2 w_{k,2}}{h_2}\right), \quad k = \alpha, \beta. \quad (18)$$

Eliminating the pressure from the Stokes's Eqs. (3) provides an extensive expression of the vorticity vector for both phases, $\nabla \times \nabla \times \mathbf{w}_k = \mathbf{0}$, ($k = \alpha, \beta$), giving a set of second-order partial differential equations for the vorticity components,

$$\frac{h_1}{r^2}\frac{\partial}{\partial x_1}\left[rh_1 h_2 \frac{\partial}{\partial x_1}\left(\frac{rw_{k,1}}{h_2}\right)\right] + \frac{h_2}{r}\frac{\partial}{\partial x_2}$$

$$\times \left[rh_1 h_2 \frac{\partial}{\partial x_2}\left(\frac{w_{k,1}}{h_1}\right)\right] - \frac{w_{k,1}}{r^2}$$

$$= 2h_2 \frac{\partial h_1}{\partial x_2}\frac{\partial w_{k,2}}{\partial x_1} - 2\left(h_1 \frac{\partial h_2}{\partial x_1} + \frac{h_1 h_2}{r}\frac{\partial r}{\partial x_1}\right)\frac{\partial w_{k,2}}{\partial x_2}$$

$$- \left\{\frac{h_1}{r^2}\frac{\partial}{\partial x_1}\left[rh_1 h_2 \frac{\partial}{\partial x_2}\left(\frac{r}{h_1}\right)\right]\right.$$

$$\left. + \frac{h_2}{r}\frac{\partial}{\partial x_2}\left(\frac{rh_1}{h_2}\frac{\partial h_2}{\partial x_1}\right)\right\}w_{k,2}, \quad k = \alpha, \beta; \quad (19a)$$

$$\frac{h_1}{r}\frac{\partial}{\partial x_1}\left[rh_1 h_2 \frac{\partial}{\partial x_1}\left(\frac{w_{k,2}}{h_2}\right)\right] + \frac{h_2}{r^2}\frac{\partial}{\partial x_2}$$

$$\times \left[rh_1 h_2 \frac{\partial}{\partial x_2}\left(\frac{w_{k,2}}{h_1}\right)\right] - \frac{w_{k,2}}{r^2}$$

$$= 2h_1 \frac{\partial h_2}{\partial x_1}\frac{\partial w_{k,1}}{\partial x_2} - 2\left(h_2 \frac{\partial h_1}{\partial x_2} + \frac{h_1 h_2}{r}\frac{\partial r}{\partial x_2}\right)\frac{\partial w_{k,1}}{\partial x_1}$$

$$- \left\{\frac{h_2}{r^2}\frac{\partial}{\partial x_2}\left[rh_1 h_2 \frac{\partial}{\partial x_1}\left(\frac{r}{h_2}\right)\right]\right.$$

$$\left. + \frac{h_1}{r}\frac{\partial}{\partial x_1}\left(\frac{rh_2}{h_1}\frac{\partial h_1}{\partial x_2}\right)\right\}w_{k,1}, \quad k = \alpha, \beta. \quad (19b)$$

We now reformulate the boundary conditions in (x_1, x_2, ϕ) coordinates. At the infinity point, $x_1 = 0$, $x_2 = -1$, the fluid is at rest, i.e.,

$$\nu_{\beta,\phi} = 0, \quad w_{\beta,1} = 0, \quad w_{\beta,2} = 0. \quad (20)$$

As we explained in Sec. II A, contact line pinning forbids rolling motion, from which Eq. (2) results. In (x_1, x_2) space, this leads to specific conditions along the left, right, and top boundaries of the rectangular domain [see Fig. 2(b)]. For the particle surface, $x_1 = -\delta$ and $x_1 = \pi - \delta$, we obtain

$$\nu_\phi = V + \omega(z_p - d), \quad k = \alpha, \beta, \quad (21a)$$

$$w_{k,1} = \pm \omega \frac{r_p}{a}, \quad k = \alpha, \beta, \quad (21b)$$

$$h_1 \frac{\partial \nu_{k,\phi}}{\partial x_1} + 2w_{k,2} = \pm \omega \frac{z_p - d}{a}, \quad k = \alpha, \beta. \tag{21c}$$

In Eqs. (21), the sign ''+'' refers to the part of the particle surface in contact with phase α. In this case, the derivative in Eq. (21c) is taken at $x_1 = \pi - \delta$. The sign ''−'' refers to the β part, $x_1 = -\delta$. The trace of the contact line which was a couple of points in the (y,z) representation, transforms into a line $(x_2 = 0)$ in toroidal coordinates. Along this line, the above condition gives

$$\nu_{k,\phi} = V - \omega d, \quad k = \alpha, \beta, \tag{22a}$$

$$w_{k,2} \sin(x_1 + \delta) - w_{k,1} \cos(x_1 + \delta) = \omega \sin \delta, \quad k = \alpha, \beta, \tag{22b}$$

$$4w_{k,1} - \frac{1}{b} \frac{\partial \nu_{k,\phi}}{\partial x_2} = 2\omega \sin x_1, \quad k = \alpha, \beta. \tag{22c}$$

At the axis of revolution $(x_2 = -1)$, Eq. (9) yields

$$\frac{\partial \nu_{k,\phi}}{\partial x_2} = 0, \quad w_{k,1} = 0, \quad \frac{\partial w_{k,2}}{\partial x_2} = 0, \quad k = \alpha, \beta. \tag{23}$$

The no-mass-transfer condition, Eq. (5), at the interface, $x_1 = \psi$, transforms into

$$\nu_{k,\phi} = u_\phi, \quad w_{k,1} = w_{i,1},$$

$$h_1 \frac{\partial \nu_{k,\phi}}{\partial x_1} + h_1 \frac{\partial \ln r}{\partial x_1} u_\phi + 2w_{k,2} = 0, \quad k = \alpha, \beta, \tag{24}$$

where $w_{i,1}$ is the x_1-component of the vorticity at the interface. After some tedious calculations to reformulate the tangential components of the dynamic boundary condition at the interface, Σ_i, Eqs. (6)–(8), we obtain for the interface velocity,

$$\frac{1}{x_2^2 h_1} \left[\eta_\beta \frac{\partial \nu_{\beta,\phi}}{\partial x_1} - \eta_\alpha \frac{\partial \nu_{\alpha,\phi}}{\partial x_1} - \frac{\partial \ln r}{\partial x_1} (\eta_\beta - \eta_\alpha) u_\phi \right]$$

$$= (\eta_s^{\mathrm{dil}} + \eta_s^{\mathrm{sh}}) \left[\frac{\partial^2 u_\phi}{\partial x_2^2} + \left(1 + \frac{\partial \ln h_1}{\partial \ln x_2} + 3 \frac{\partial \ln r}{\partial \ln x_2} \right) \frac{1}{x_2} \frac{\partial u_\phi}{\partial x_2} \right.$$

$$\left. - \frac{2 \sin^2 x_1}{b^2 h_2^2} u_\phi \right] + 2 \eta_s^{\mathrm{sh}} \left(\frac{1}{x_2} \frac{\partial \ln r}{\partial x_1} \right)^2 u_\phi$$

$$- 2 \eta_s^{\mathrm{dil}} \frac{1}{h_2} \frac{\partial w_{i,1}}{\partial x_2} - 4 (\eta_s^{\mathrm{sh}} + \eta_s^{\mathrm{dil}}) \frac{1}{h_2} \frac{\partial \ln r}{\partial x_2} w_{i,1}, \tag{25a}$$

and for the interfacial vorticity,

$$\frac{1}{x_2^2 h_1} \left[\eta_\beta \frac{\partial w_{\beta,1}}{\partial x_1} - \eta_\alpha \frac{\partial w_{\alpha,1}}{\partial x_1} + \frac{\partial \ln h_1}{\partial \ln x_2} (\eta_\beta w_{\beta,2} - \eta_\alpha w_{\alpha,2}) \right]$$

$$= \eta_s^{\mathrm{sh}} \left\{ \frac{\partial^2 w_{i,1}}{\partial x_2^2} + \left(1 + \frac{\partial \ln h_1}{\partial \ln x_2} + \frac{\partial \ln r}{\partial \ln x_2} \right) \frac{1}{x_2} \frac{\partial w_{i,1}}{\partial x_2} \right.$$

$$\left. - \left[\frac{4}{(1 - x_2^2)^2} - \frac{2 \sin^2 x_1}{b_2 h_2^2} \right] w_{i,1} \right\}. \tag{25b}$$

D. Numerical procedure

Equations (18) and (19) with the imposed boundary conditions Eqs. (20)–(25), are solved numerically applying the basic ideas of the Alternating-Direction-Implicit (ADI) method (see, e.g., Ref. 24). The latter was already employed[19] for solving the problem of the motion of a particle in a thin liquid film. The approach implies introducing an artificial time variable followed by a time iteration procedure (see Ref. 19 for details). Each step provides an intermediate set of numerical values for the pressure and velocity fields. The time iteration is repeated until stationarity is reached.

To compute the drag force, **F**, and torque, **M**, acting on the particle, we use the following relationship:[11,25]

$$\mathbf{F} = \int_{\Sigma_{p,\alpha}} \mathbf{P}_\alpha \cdot \mathbf{n}_{p,\alpha} d\Sigma + \int_{\Sigma_{p,\beta}} \mathbf{P}_\beta \cdot \mathbf{n}_{p,\beta} d\Sigma + \int_{L_c} \mathbf{P}_i \cdot \mathbf{n}_c dL, \tag{26a}$$

$$\mathbf{M} = a \int_{\Sigma_{p,\alpha}} \mathbf{n}_{p,\alpha} \times \mathbf{P}_\alpha \cdot \mathbf{n}_{p,\alpha} d\Sigma + a \int_{\Sigma_{p,\beta}} \mathbf{n}_{p,\beta}$$

$$\times \mathbf{P}_\beta \cdot \mathbf{n}_{p,\beta} d\Sigma + a \int_{L_c} \mathbf{n}_c \times \mathbf{P}_i \cdot \mathbf{n}_c dL, \tag{26b}$$

where $\mathbf{n}_{p,\alpha}$ and $\mathbf{n}_{p,\beta}$ are the unit vectors normal to surfaces $\Sigma_{p,\alpha}$ and $\Sigma_{p,\beta}$, correspondingly. L_c is the three-phase contact line and $\mathbf{n}_c$ is the unit vector perpendicular to it. The first two terms on the right-hand side of Eq. (26) account for the friction experienced by the particle from the bulk phases, while the last term brings in the additional hydrodynamical resistance from the interface Σ_i. **F** is proportional to **V** and because of the symmetry of the problem the torque **M** has only an x-component i.e., $M_y = 0$ and $M_z = 0$. The computed quantities are the particle drag coefficient, f, and the particle torque coefficient, m, defined by

$$\mathbf{F} = f\mathbf{V}, \tag{27a}$$

$$\mathbf{M} = maV\mathbf{e}_x. \tag{27b}$$

We compute reduced coefficients: $\bar{f} = f/f_0$, where $f_0 = 6\pi \eta_\alpha a$ is the Stokes drag coefficient in phase α and $\bar{m} = m/m_0$, where $m_0 = 8\pi \eta_\alpha a$ is the Kirchoff's rotation torque coefficient in phase α. Input parameters of the computation are: the viscosity ratio, η_β / η_α, the shear and dilational viscosity numbers,

$$E = \frac{\eta_s^{\mathrm{sh}}}{a \eta_\alpha} \quad \text{and} \quad K = \frac{\eta_s^{\mathrm{dil}}}{a \eta_\alpha}, \tag{28}$$

the size ratio, R/a, and the scaled penetration depth, $\bar{d} = d/a$ (for $\bar{d} = -1$ the particle is completely immersed in the enclosed phase α and for $\bar{d} = 1$ in phase β). The numerical code is written in FORTRAN and usually run on a PC Pentium-MMX computer. The program is made of four modules. The first module starts with a coarse periodic sampling of the (x_1, x_2) domain and calculates the values of the ϕ-component of the velocity and the w_1 and w_2 components of the vorticity vector. The following modules work with increasing sampling densities and provide increasingly accurate velocity fields. The final module assures a precision of about 0.02% for the calculated velocity values (there is no essential difficulty for increasing the precision by using more powerful machines). However the drag and torque coeffi-
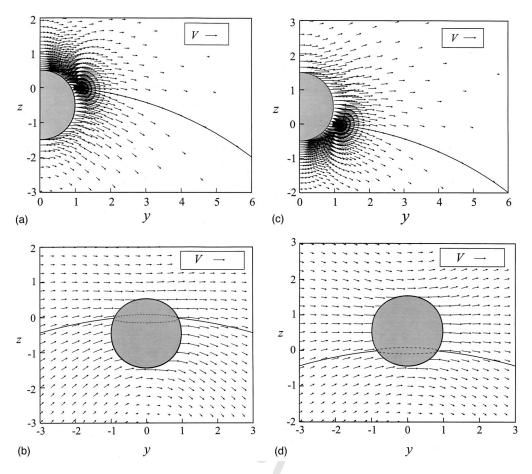
FIG. 3. Velocity field in the $x=0$ plane (distances are scaled to particle radius) for a spherical particle moving in y-direction with velocity V; $\eta_\alpha/\eta_\beta=1$, $E=0$, $K=0$, $R/a=10$. In (a) and (b) $\bar{d}=-0.5$, in (c) and (d) $\bar{d}=0.5$; (a) and (c) present the velocity distribution in a (x_1,x_2) lattice, the gray hemisphere represents the particle, and the dotted line denotes the interface position. The $x_1=$ const and $x_2=$ const circles can be recognized as the loci of the velocity field vectors' origins. (b) and (d): same numerical data in Cartesian lattice, the solid line denotes the interface position. The broken curve represents the contact line (in perspective, artificially).

cients are computed with lower precision ($\pm1\%$) because of the integrations in Eq. (26). The computing time depends on the values of the input parameters and on the required numerical accuracy. For typical inputs such as $\eta_\alpha/\eta_\beta=1$, $E=2$, $K=0$, $R/a=5$, and $\bar{d}=0$, it takes about 2 h to compute $\bar{f}$ and $\bar{m}$ with the highest precision. Bringing $\bar{d}$ close to ±1 demands increasing the (x_1,x_2) sampling density and makes computation several times longer. When $\bar{d}=\pm1$, the set of circles corresponding to $x_2=constant$ [see Eq. (12b)] collapses to the origin ($r=0$, $z=0$), i.e., to the particle-VDB contact point. Because of this limitation, the numerical procedure is inapplicable to the case of a particle tangent to the interface. The numerical results presented in the following section were obtained by running the program on a PC-Pentium II computer. The maximum computation time was limited to about 50 h, which imposed a limitation of the particle position to $|\bar{d}| \geqslant 0.9$. This corresponds to a contact angle [θ, see Fig. 1(b)] between 25 and 155°.

III. NUMERICAL RESULTS AND DISCUSSION

A. Inviscid spherical interface. Recirculation effect

To visualize the events occurring as a consequence of the particle motion along the interface, we calculated the (Oy,Oz) profile of the velocity field in the $x=0$ plane for two different penetration depths of the particle. Figure 3(a) shows the result for a *nonviscous interface* ($E=K=0$) and for similar α and β phases ($\eta_\alpha/\eta_\beta=1$). In Figs. 3(a) and 3(b) the particle strongly penetrates into the VDB interior ($\bar{d}=-0.5$) while in Figs. 3(c) and 3(d) the penetration is weak ($\bar{d}=0.5$). The size ratio, R/a, is everywhere$=10$. The particle is presented in gray and the dotted curve is the spherical interface, Σ_i. Because of the symmetry in the velocity field, $v(x,y,z)=-v(x,-y,z)$, it is sufficient to show only the $y>0$ side. In Figs. 3(a) and 3(c) the representation corresponds to a periodic sampling of the (x_1,x_2) domain, while in Figs. 3(b) and 3(d) a standard grid in the (y,z) plane is used. Note that (x_1,x_2) sampling ensures a high mapping density of the region close to the particle surface, and thus optimizes the accuracy in the velocity field entering Eq. (26).

The range of the perturbation caused by the particle motion is readily seen in Figs. 3(b) and 3(d). At large distances in the continuous phase, β, the velocity drops down to zero (undisturbed fluid). The influence of the solid particle is not very far reaching. At distances of six times the particle radius, the velocity in the y-direction is less than $0.2V$, whereas in the z-direction the velocity profile is quickly damped down to the same value already at distances less
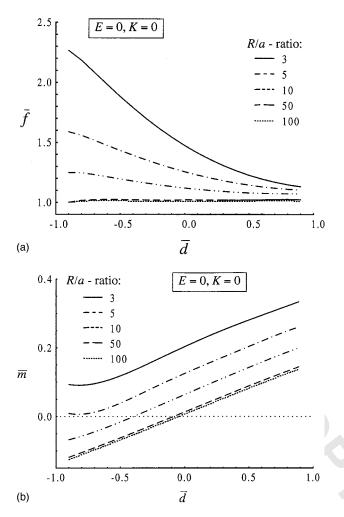
(a)

(b)

FIG. 4. Size ratio effect for a nonviscous interface ($E=0$, $K=0$). Dimensionless drag coefficient $\bar{f}$ (a) and torque coefficient $\bar{m}$ (b), as a function of penetration depth, $\bar{d}$, for different size ratios, R/a (see the insert), $\eta_\alpha/\eta_\beta = 1$.

than a particle diameter, see Figs. 3(b) and 3(d). When choosing zero interface viscosity numbers (nonviscous interface) we want to emphasize the effect of just the finite size of the VDB. The spherical shell, Σ_i, plays the role of a wall blocking the flow lines which are forced to follow its contour. The flow in α phase is looped inside the finite volume encompassed by the interface. This is an example of "recirculation," similar to that encountered in the problem of the motion of a particle in a closed box.[26] This recirculation is most pronounced when the particle is more deeply immersed in the enclosed phase, $\bar{d} = -0.5$ [see Fig. 3(b)]. The less the particle portion in phase α, the weaker the perturbation (recirculation).

Figure 4 shows the incidence of the flow confinement on the value of the particle drag and torque. In Fig. 4(a), the dimensionless friction coefficient, $\bar{f}$, is plotted as a function of the scaled penetration depth, $\bar{d}$, for systems with different size ratios, R/a. Again the surface viscosity is chosen to be zero ($E=0$, $K=0$). The lower limit for $\bar{f}$ is just 1 ($f=f_0$). This limit is approached for large size ratios [$R/a \approx 50$ in Fig. 4(a)] when the particle feels the interface as flat and infinite. When the VDB size is decreased to ten times the

size of the particle, the finite volume effect becomes distinctly pronounced. The behavior of $\bar{f}$ is as expected: the deeper the particle penetration, the larger the friction ratio. Even at weak penetration ($\bar{d}=0.9$), where a very small portion of the particle (about 8% for $R/a=10$) is in the enclosed phase α, we observe a noticeable increase in $\bar{f}$. The behavior of the dimensionless torque coefficient $\bar{m}$ is illustrated in Fig. 4(b). All other parameters are the same as in Fig. 4(a). For large size ratios, R/a, the torque coefficient is symmetric with respect to the particle penetration depth. When the membrane is flat ($R/a \gg 1$), the particle performs a pure translational motion. When $d>0$ (see Fig. 1), the hydrodynamic torque tends to make the particle rotate counterclockwise. We find the same sense for the torque as that found by Lee and Leal[28] for a particle close to but not in contact with a plane interface ($\bar{d}>1$). Following Lee and Leal,[28] we define the torque as positive in this case.

Of course, the particle rotation is forbidden by the contact-line-pinning condition, as we explained in Sec. II A. In other words, the hydrodynamic torque is counteracted by a mechanical torque from the membrane at the level of the contact line. When the size ratio decreases, the particle performs a rotational motion as well, whose angular velocity is given by Eq. (1). Because of this rotation, the flow velocity around the upper part of the particle is larger than around the bottom part (see the flow fields in Fig. 3). This has the consequence of making the torque more positive, whatever the particle's penetration. When $R/a<5$, the torque becomes positive for all penetrations. For intermediate size ratios, e.g., $R/a=10$, the torque is negative only when $\bar{d}<-0.4$, i.e., when the particle is largely inside the VDB [for instance, as in Fig. 3(a)].

Note that $|\bar{m}|$ is everywhere moderate (<0.35), which means that the computed values of the torque are definitely less than $3\pi\eta a^2 V$ in absolute value. As discussed in the Appendix, such torques cannot definitely distort the VDB shape in usual experimental conditions with lipid vesicles.

B. Flat infinite interface. Comparison with Saffman's disc problem

When $R/a \to \infty$, finite-size effects obviously disappear. Analyzing the problem for a flat interface simply amounts to choosing $\psi=0$ [see Fig. 1(a)]. We calculated the drag and torque coefficients for three different values of the surface viscosity, again supposing $\eta_\alpha = \eta_\beta$. The data are presented in Fig. 5. Each of the curves is symmetrical about $\bar{d}=0$ because of the symmetry of the system about the interface Σ_i. In the case of an inviscid interface ($E=0$, $K=0$), the only factor influencing the friction is the particle position, i.e., $\bar{d}$. The base curve for the drag coefficient in Fig. 5(a) (dotted line) has its minimum at $\bar{d}=0$ when the sphere equator is located in the interface plane. In this situation, the streamlines are identical to those for the same particle in the bulk fluid; then $f=f_0=6\pi\eta a$, the sphere Stokes friction. When $\bar{d}\neq0$, the interface perturbs the streamlines of the Stokes flow and this results in increasing the friction. This explains why the bottom curve in Fig. 5(a) is concave. Con-
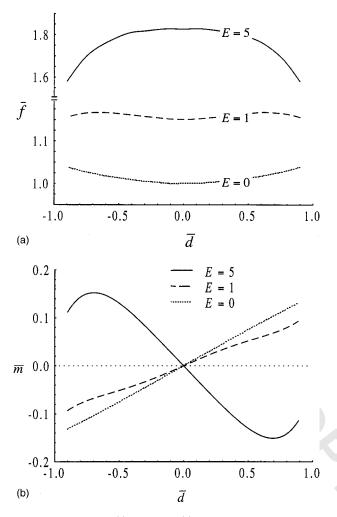
FIG. 5. Reduced friction (a) and torque (b) of a spherical particle across a flat interface $K=0$ and $\eta_\alpha/\eta_\beta=1$. The dotted line corresponds to a nonviscous interface, $E=0$; the broken and solid lines to $E=1$ and $E=5$, respectively.

versely, when the interface is very viscous ($E=5$, solid line), the curve becomes convex. Here the drag coefficient is mainly influenced by the interface friction rather than by hydrodynamic perturbations in bulk phases. The drag coefficient arrives at a maximum when $\bar{d}=0$. In that position the intersection area of the particle with the viscous surface is the largest ($b=a$), which leads to a greater resistance. In general, the sphere drag coefficient may be decomposed as $f=f_0+f_{\rm exc}$, where $f_{\rm exc}$ is an excess friction. The decomposition gets a simple physical significance when the interface viscosity is large ($E\gg1$). In this limit, $f_{\rm exc}$ essentially represents the friction which the interface opposes to the motion of the contact line, in other words of the disc (of radius b) which the particle intercepts in the interface plane. When $E\sim1$, $f_{\rm exc}$ is influenced by both the streamlines' perturbation in bulk phases and by the plane disc friction. Because of the competition between these two mechanisms, the $\bar{f}(\bar{d})$ curve evolves from concave to convex when $|\bar{d}|$ increases [Fig. 5(a), $E=1$]. Results for the hydrodynamic torque acting on the particle are shown in Fig. 5(b). Because the membrane is supposed flat, all curves are odd in $\bar{d}$. Note that $|\bar{m}|<0.35$ when $E<5$, which again means that the torque is definitely

less than m_0, the Kirchoff's value corresponding to an angular velocity equal to V/a. The 3D fluids on both sides of the membrane are supposed identical, as before (results for water/air interface are given in Ref. 11).

The curve corresponding to $E=0$ is the same as that in Fig. 4(b) in the infinite R/a limit. When $d>0$, the flow wants to make the particle rotate counterclockwise, i.e., $\bar{m}$ is positive. When the membrane viscosity increases, so does the friction on the side of the particle in contact with the membrane. Then ($d>0$ and E very large) the interfacial friction tends to make the particle rotate clockwise. If E is large enough, the torque becomes negative. The influence of the interfacial friction has a maximum at some finite penetration depth, $\bar{d}$ (about ±0.7 for $E=5$). Beyond $\bar{d}$, $|\bar{m}|$ decreases because the size of the contact line rapidly decreases.

It is interesting to compare the friction of the spherical particle to that of a disc with the same contact line. Thus we come back to Saffman's problem, for a disc of radius b and same thickness as that of the membrane. Saffman's equation for the disc friction coefficient reads

$$f_{\rm disc}=\eta_s^{\rm sh}\frac{4\pi}{\ln\left(\dfrac{l}{b}\right)-\gamma},\qquad(29)$$

where l is a characteristic length, γ is Euler's constant ($=0.5772...$). In the standard situation of an infinite membrane inside a continuous phase of bulk viscosity η, $l=\eta_s^{\rm sh}/\eta$ (we recall that the shear surface viscosity has the dimension of a bulk viscosity$\times$length). Equation (29) is valid when $b/l\ll1$ (there is no such restriction in the generalized theory of Hughes et al.[4]). The important and somewhat counterintuitive idea conveyed by Eq. (29) is that the disc friction depends only marginally on its size. Because b intervenes only through a logarithm, $f_{\rm disc}$ remains on the order of $\eta_s^{\rm sh}$, whatever b. Our analysis for low viscosity numbers, see Fig. 4(a) ($E<2$), also demonstrates a very weak dependency of the spherical particle drag coefficient on the particle penetration, or equivalently, on the radius of the disc, b, that the particle intercepts in the membrane. This analogy with Saffman's disc problem suggests that the spherical particle excess friction follows an equation similar to Eq. (29),

$$f_{\rm exc}=\eta_s^{\rm sh}g\left(\frac{l}{b}\right),\qquad(30)$$

where g is a slowly varying function; Eq. (29) is equivalent (for $\eta=\eta_\alpha=\eta_\beta$) to

$$\bar{f}_{\rm exc}\equiv\bar{f}-1=\frac{E}{6\pi}g\left(\frac{E}{\sin\theta}\right).\qquad(31)$$

In Fig. 6 the reduced excess friction $\bar{f}_{\rm exc}/E$ is plotted versus $E/\sin\theta$. The broken line was computed for a constant angle $\theta=90°$ ($\bar{d}=0$) and $1\leqslant E\leqslant100$. The gray zone marks the numerical error band for the computed data. We do find a slowly varying function, which can be approximated by a power low (solid line) with a very weak exponent,

$$g(x)\approx2.93x^{-0.116}\quad(\theta=90°,1\leqslant x\leqslant100).\qquad(32)$$
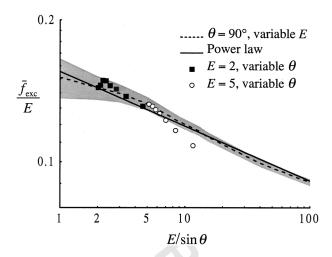
FIG. 6. Scaled excess friction $\bar{f}_{\text{exc}}/E$ versus $E/\sin\theta$ for a flat infinite membrane. See text and figure insert for definition of symbols. The gray band represents the estimated uncertainty of the computed values of $\bar{f}_{\text{exc}}/E$. As the relative uncertainty of $\bar{f}$ is about constant, that of $\bar{f}_{\text{exc}}/E$ diverges when $\bar{f}\rightarrow 1$, i.e., when $E\rightarrow 0$.

FIG. 7. Dimensionless drag coefficient, $\bar{f}$, as a function of penetration depth, $\bar{d}$, for different size ratios, R/a, and shear surface viscosity numbers; $K=0$, $\eta_{\alpha}/\eta_{\beta}=1$. The dotted curve corresponds to $E=0$ (the numerical data are the same as in Fig. 4, see legend). The three upper curves present results for $E=2$.

This power low fits to the computed values within numerical error. Equations (30)–(32) show that $f_{\text{exc}}\approx 2.9\eta_s^{\text{sh}}$ for $a=l$ and only decreases down to $1.4\eta_s^{\text{sh}}$ for $a=0.01l$. Note that Eq. (32) only holds for $\theta=90°$ ($\bar{d}=0$). We thus find that the excess friction of a macroscopic spherical particle whose center lies in the membrane plane ($\theta=90°$) behaves similarly to the disc friction in Saffman's theory. Nevertheless note that the similarity is only qualitative [Eqs. (28) and (32) are quantitatively different], which means that Saffman's equation, Eq. (29), cannot be used to interpret data with macroscopic spherical particles.[27] In their most general form (with variable θ), Eqs. (30) and (31) suggest that the dependence of f_{exc} on b might be universal, i.e., independent of the contact angle. If it were so, increasing the particle size while increasing $|d|$ so as to keep $b=a\sin\theta=$constant should not significantly modify f_{exc}. For instance, a small sphere, $a=1$ μm, $\theta=90°$, and a large one, $a=3$ μm, $\theta=20°$, should have the same friction. We tested this conjecture for $E=2$ and $E=5$ and found that it was valid within the error band only for angles not too far from 90°, say $45°\leqslant\theta\leqslant 135°$. For small (or large, symmetrically) contact angles, the particle friction is inferior to that for $\theta=90°$, at constant b. In fact, this difference is not surprising; coming back to the above given example, it is clear that the velocity fields corresponding to the small and large spheres are necessarily different and so are the particle frictions. Nevertheless, this difference becomes negligibly small when $|d|<0.7$.

As we discussed before, our procedure does not allow us to compute the particle drag coefficient in the $\bar{d}=\pm 1$ limit, i.e., when the particle is tangent to the interface. Nevertheless, when the viscosity is not too large $\bar{f}(\bar{d}=\pm 1)$ can be found by extrapolating the $\bar{f}(\bar{d})$ curve. For instance, we find $\bar{f}(\bar{d}=\pm 1)\cong 1.05$ for a nonviscous interface ($E=0$) between two fluids of equal viscosities ($\eta_{\alpha}=\eta_{\beta}$). Interestingly, the $\bar{d}=\pm 1$ configuration can be found as a limit situation too, in the case of a sphere near to, but not in contact with a flat
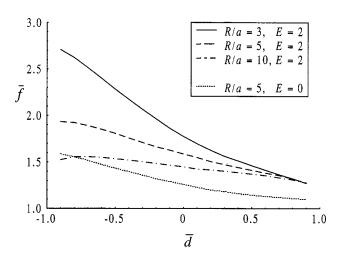
interface. A numerical exact solution to this problem was worked out by Lee and Leal[28] for a nonviscous interface; recently the same problem was generalized to a flat viscous interface by Danov et al.[29] The sphere tangent to the interface configuration corresponds to the $\bar{d}=1$ limit in Lee and Leal's notation. Their result for $\lambda=\eta_{\alpha}/\eta_{\beta}=1$ is $\bar{f}(\bar{d}=1)\cong 1.051$, which is in agreement with ours. We checked that this agreement remained true with viscous films ($E\leqslant 2$) using data from Danov et al.[29]

C. General situation: Spherical viscous interface

Having discussed the limit situations of a finite-size inviscid interface and that of flat infinite viscous interface, we now come to the general problem of a spherical viscous interface. Making the interface viscous obviously increases the particle friction. For a large number of systems to which the problem relates, the dilational and the shear surface viscosities are of the same order of magnitude. It is quite common that they differ by a factor of 0.2 up to 5. Conversely, for biological membranes η_s^{dil} and η_s^{sh} differ by several (4–5) orders of magnitude.[30] Since this work is mainly dedicated to lipid membranes,[12,31] we will put $K=0$. Figure 7 presents numerical data for four systems with different parameters indicated in the legend. For the three upper curves the surface shear viscosity number is $E=2$ and R/a varies between 3 and 10. To facilitate the comparison, the base curve presents numerical results ($E=0$, $R/a=5$) already displayed in Fig. 4(a). The main feature in Fig. 7 is the upward shift of the friction values (for $R/a=5$) in the whole interval of $\bar{d}$. The effect is noticeable even for penetrations corresponding to $\bar{d}=0.9$ or $\bar{d}=-0.9$ when the size of the disc, b, which the particle intercepts in the interface is $\leqslant a$. However, the viscosity influence for $E=2$ does not overpower the finite-size contribution and as a whole the curves preserve their negative slope tendency. An interesting point to note is that all three upper curves converge to one and the same value for
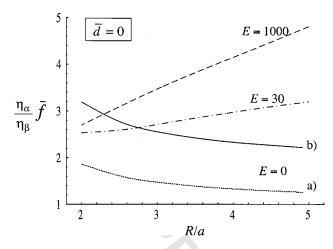
FIG. 8. Friction coefficient scaled to Stokes resistance for phase β. $K=0$, $\bar{d}=0$. The two upper curves present results for high shear surface viscosity ($E=30$ and $E=1000$) and a viscosity ratio $\eta_\alpha/\eta_\beta=1$. The dotted line, curve (a), corresponds to a nonviscous surface, $E=0$ and $\eta_\alpha/\eta_\beta=1$, while the solid line, curve (b), is calculated for $E=0$ and $\eta_\alpha/\eta_\beta=1.5$.

FIG. 9. Velocity field for a particle on a very viscous interface ($E=30$). Input parameters are $\eta_\alpha/\eta_\beta=1$, $K=0$, $R/a=3$, $\bar{d}=0$. The velocity field is shown in toroidal coordinates lattice presentation. The dotted line shows the position of the spherical interface.

small penetrations ($\bar{d}=0.9$), in contrast to the behavior observed with the inviscid membrane, $E=0$ [see Fig. 4(a)]. Obviously, in this region the interface viscosity dominates the flow confinement effect.

Figure 8 shows results for high shear viscosity numbers. The friction coefficient is plotted as a function of the size ratio, R/a, of the VBD-particle complex. Here we consider the general situation where α and β may be different, and plot $(\eta_\alpha/\eta_\beta)\bar{f}$. In other words the friction coefficient presented in the figure is scaled by the Stokes friction not in phase α as in the previous figures, but in phase β. Only for curve b, solid line, the viscosity ratio is different from 1: $\eta_\alpha/\eta_\beta=1.5$. For all curves $\bar{d}$ is set$=0$. The novel effect in the figure is the growth of the friction for large E (two upper curves) when the size ratio increases. We recall that for small values of the shear viscosity ($E=2$), $\bar{f}$ is a decreasing function of R/a (see Fig. 7). Figure 8 demonstrates an opposite behavior when E is very large. The interpretation of this apparently paradoxical result lies in the possibility of the VDB-particle complex to rotate as a whole in β phase. In the limit of an infinite membrane viscosity, the VDB-particle complex may be viewed as a rigid body. The friction involved in the particle motion is then the rotational friction of the whole complex in β phase. Obviously, this friction increases when R increases. The upper limit of $\bar{f}$ for $\bar{d}\to-1$ may be estimated from the Kirchoff equation[25,32] for a rotating sphere; both upper curves on the figure are below that limit. We find:[32] $\bar{f}\to4R/3a$ when $\eta_s\to\infty$. The overall rotating effect acts oppositely to the above described recirculation effect. The influence of the latter is obviously more pronounced for ''less rigid'' (less viscous) surfaces. The dotted line, curve a, $E=0$, $\eta_\alpha/\eta_\beta=1$, represents the extreme case of an inviscid interface for identical α and β phases. The lower limit of the curve at infinity is set by the net Stokes' resistance ($\bar{f}=1$). Curve b, solid line ($\eta_\alpha/\eta_\beta=1.5$, $E=0$), shows that increasing η_α results in increasing $\bar{f}$, but the general tendency of the curve is preserved as a whole.

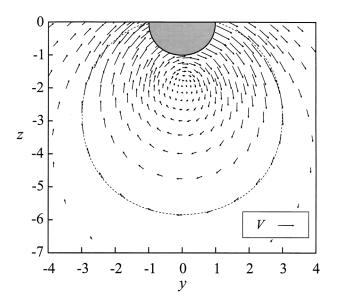The slightly positive slope of the third curve ($E=30$) in Fig. 8 indicates that both recirculation and overall rotation are operative in this case. We expect rigid rotation to be the leading mechanism for small R/a; conversely, when R is very large, rotating the VDB as a whole costs too much in terms of dissipation and it is preferable for the particle to shear the interface. Ultimately, when $R\to\infty$, we are back to the situation of an infinite interface, with obviously no overall motion. Size ratios in Fig. 8 ($2\leqslant R/a\leqslant5$) are intermediate between the $R\to0$ and $R\to\infty$ regimes. For illustration, the flow field corresponding to $E=30$, $R/a=3$, $\eta_\alpha=\eta_\beta$, is shown in Fig. 9, in toroidal coordinates representation. The existence of a partial overall rotation of the system is evident from the slow decrease of the velocity along the interface; compare with Figs. 3(a) and 3(b). However, note that the flow pattern inside the VDB is not cylindrical (the vortex is not located at about mid-distance between the particle and the VDB center and follows the particle motion), which means that part of the dissipation takes place in the VDB interior.

IV. CONCLUSIONS

The theoretical study presented in this work was aimed at assessing the friction coefficient for systems where the curvature of the interface influences the resistance experienced by the floating particle. The model refers to slow motion in the Stokes' regime and small capillary numbers and is applicable both to curved and flat interfaces. The approach accounts for the viscous properties of the surface.

A toroidal coordinate system was introduced allowing decoupling of the coordinate variables. The hydrodynamic equations and boundary conditions were transformed following the two-vorticity-one-velocity formalism, which allowed us to eliminate the ϕ-coordinate, thus reducing the problem

to a two-variable one. The numerical solution was achieved employing the Alternating-Direction-Implicit method with a second-order precision.

The performed analysis on the influence of different factors demonstrated a considerable contribution to the friction coefficient both from the finite size of the enclosed fluid and from the surface shear viscosity. An interesting prediction of the numerical calculations is the possible rotation of the particle/interface complex as a whole when surface viscosity is increased, i.e., when the particle is blocked on the spherical shell.

Finally, the theory makes feasible the interpretation of experiments based on the ''falling ball viscosimetry'' method independently of the size ratio of the vesicle/particle complex.[31] Moreover, the approach is applicable to systems where the fluids on both sides of the interface are of different viscosities. This happens in emulsions stabilized by solid particles (so-called Pickering emulsions).

APPENDIX: DOES THE PARTICLE MOTION PERTURB THE SHAPE OF THE INTERFACE?

Since we supposed a spherical VDB, we implicitly assumed that the particle motion would not modify the shape of the interface. We expect this assumption to be approximately valid whenever the capillary number, $Ca = \eta V/\sigma$, is much inferior to 1. Here σ is the interfacial tension. Roughly, Ca represents the ratio of the friction force, F, to the surface tension force, F_{cap}, acting on the particle. As we argue in the discussion, F remains on the order of the Stokes friction ($F \propto 6\pi \eta a V$) in the bulk fluid. The capillary force is on the order of $2\pi\sigma b = 2\pi\sigma\sqrt{a^2 - d^2}$. We thus find the above result for Ca whenever $|d|$ is not close to a, i.e., when the particle is well across the interface. Equivalently, Ca represents the ratio of the viscous torque ($\propto \eta a^2 V$) to the capillary torque ($\propto \sigma b a$) acting on the particle. To estimate Ca in typical conditions, we may put $V \propto (2/9)a^2\Delta\rho g/\eta$, the particle sedimentation velocity in the bulk fluid. With polystyrene spheres in water and $a \cong 5\,\mu$m (this corresponds to the experiments in Dietrich et al.[29]), ηV is of the order of 10^{-5} dyn/cm. Correspondingly small values of the interfacial tension exist only with so-called ''quasi-spherical'' vesicles, whose shapes are fluctuating under thermal agitation.[33] Vesicles with no visible thermal fluctuations have tensions at least of the order of 0.1 dyn/cm.[30] In conclusion, a vesicle (or a VDB in general) which appears spherical under the microscope, corresponds to $Ca \ll 1$. Strictly speaking, this condition cannot remain valid when $|d| \cong a$, i.e., when the contact line reduces to a point ($b \to 0$). However, the value of Ca is definitely increased only

when b is extremely small, which means d/a very close to ± 1. As we explain in Sec. II B, the mapping of the (r,z) plane by toroidal coordinates fails in the $\bar{d} \to \pm 1$ limit. For this reason, the accuracy of the numerical procedure considerably decreases when the size of the contact line becomes small compared to a. Keeping the computing time within reasonable limits ($\cong 50$ h), the friction coefficient can be computed within about $\pm 1\%$ only when $b > 0.1a$. In such conditions, Ca is not considerably larger than $\eta V/\sigma$, and, consequently, the above estimate for the validity of the theory remains in force. In other words, there is no risk that a computed value of the particle drag coefficient be physically wrong because the interface shape could be distorted by the particle motion.

[1]D. E. Tambe and M. M. Sharma, ''The effect of colloidal particles on fluid-fluid interfacial properties and emulsion stability,'' Adv. Colloid Interface Sci. **52**, 1 (1994).

[2]P. G. Saffman and M. Delbrück, ''Brownian motion in biological membranes,'' Proc. Natl. Acad. Sci. U.S.A. **72**, 3111 (1975).

[3]P. G. Saffman, ''Brownian motion in thin sheets of viscous fluid,'' J. Fluid Mech. **73**, 593 (1976).

[4]B. D. Hughes, B. A. Pailthorpe, and L. P. White, ''The translational and rotational drag on a cylinder moving in a membrane,'' J. Fluid Mech. **110**, 349 (1981).

[5]J. F. Klinger and H. M. McConnell, ''Brownian motion and fluid mechanics of lipid monolayer domains,'' J. Phys. Chem. **97**, 6096 (1993).

[6]R. M Clegg and W. L. C. Vaz, ''Translation diffusion of proteins and lipids in artificial lipid bilayer membranes. A comparison of experiment with theory,'' in *Progress in Protein-Lipid Interactions* (Elsevier, New York, 1985), Vol. 1.

[7]W. L. C. Vaz, F. Goodsaid-Zalduondo, and K. Jacobson, ''Lateral diffusion of lipids and proteins in bilayer membranes,'' FEBS Lett. **174**, 199 (1984).

[8]H. A. Stone and A. Ajdari, ''Hydrodynamics of a particle embedded in a flat surfactant layer overlaying a subphase of finite depth,'' J. Fluid Mech. **369**, 151 (1998).

[9]J. T. Petkov, N. D. Denkov, K. D. Danov, O. V. Velev, R. Aust, and F. Durst, ''Measurement of the drag coefficient of spherical particles attached to fluid interfaces,'' J. Colloid Interface Sci. **172**, 147 (1995).

[10]J. T. Petkov, K. D. Danov, and N. D. Denkov, ''Precise method for measuring the shear surface viscosity of surfactant monolayers,'' Langmuir **12**, 2650 (1996).

[11]K. Danov, R. Aust, F. Durst, and U. Lange, ''Influence of the surface viscosity on the hydrodynamic resistance and surface diffusivity of a large Brownian particle,'' J. Colloid Interface Sci. **175**, 36 (1995).

[12]K. Velikov, C. Dietrich, A. Hadjiisky, K. Danov, and B. Pouligny, ''Motion of a massive microsphere bound to a spherical vesicle,'' Europhys. Lett. **40**, 405 (1997).

[13]C. Dietrich, M. Angelova, and B. Pouligny, ''Adhesion of latex spheres to giant phospholipid vesicles: Statics and dynamics,'' J. Phys. II **7**, 1651 (1997).

[14]E. B. Dussan and S. H. Davis, ''On the motion of a fluid-fluid interface along a solid surface,'' J. Fluid Mech. **65**, 71 (1974).

[15]L. Landau and E. M. Lifshitz, *Fluid Mechanics* (Addison-Wesley, Reading, MA, 1960).

[16]D. A. Edwards, H. Brenner, and D. T. Wasan, *Interfacial Transport Processes and Rheology* (Butterworth-Heinemann, Washington, D.C., 1991).

[17]M. J. Boussinesq, ''The application of the formula for surface viscosity to the surface of a slowly falling droplet in the midst of a large unlimited amount of fluid which is at rest and possesses a smaller specific gravity,'' Ann. Chim. Phys. **29**, 349 (1913).

[18]L. E. Scriven, ''Dynamics of a fluid interface,'' Chem. Eng. Sci. **12**, 98 (1960).

[19]K. D. Danov, R. Aust, F. Durst, and U. Lange, ''Influence of the surface viscosity on the drag and torque coefficients of a solid particle in a thin liquid layer,'' Chem. Eng. Sci. **50**, 263 (1995).

[20]K. D. Danov, R. Aust, F. Durst, and U. Lange, ''Slow motion of a solid spherical particle close to a viscous interface,'' Int. J. Multiphase Flow **21**, 1169 (1995).

[21] K. D. Danov, R. Aust, F. Durst, and U. Lange, ''On the slow motion of an interfacial viscous droplet in a thin liquid layer,'' Chem. Eng. Sci. **50**, 2943 (1995).

[22] A. J. Goldman, R. G. Cox, and H. Brenner, ''Slow viscous motion of a sphere parallel to a plane wall,'' Chem. Eng. Sci. **22**, 637 (1967).

[23] M. E. O'Neil and K. Stewartson, ''On the slow motion of a sphere parallel to a nearby plane wall,'' J. Fluid Mech. **27**, 705 (1967).

[24] C. Pozrikidis, *Introduction to Theoretical and Computational Fluid Dynamics* (Oxford University Press, New York, 1997).

[25] J. Happel and H. Brenner, *Low Reynolds Number Hydrodynamics with Special Applications to Particulate Media* (Prentice-Hall, Englewood Cliffs, NJ, 1965).

[26] C. A. J. Fletcher, *Computational Techniques for Fluid Dynamics* (Springer-Verlag, Berlin, 1991), Vols. 1 and 2.

[27] The problem of a spherical inclusion, i.e., of a sphere whose diameter approximately matches the membrane thickness, is different. In this case, it seems reasonable to confound the particle with a disc and apply Saffman's equation. See, e.g., C. Cheung, H. Y. Hwang, X. I. Wu, and H. J. Choi, Phys. Rev. Lett. **76**, 2531 (1996).

[28] S. H. Lee and L. G. Leal, ''Motion of a sphere in the presence of a plane interface. Part 2. An exact solution in bipolar co-ordinates,'' J. Fluid Mech. **98**, 193 (1980).

[29] K. D. Danov, T. G. Gurkov, H. Raszillier, and F. Durst, ''Stokes flow caused by the motion of a rigid sphere close to a viscous interface,'' Chem. Eng. Sci. **53**, 3413 (1998).

[30] E. Evans and D. Needham, ''Physical properties of surfactant bilayer membranes: Thermal transitions, elasticity, rigidity, cohesion, and colloidal interactions,'' J. Phys. Chem. **91**, 4219 (1987).

[31] R. Dimova, C. Dietrich, K. Danov, A. Hadjiiski, and B. Pouligny, ''Falling ball viscosimetry of giant vesicle membranes: Finite-size effects,'' Eur. Phys. J. B (in press).

[32] G. Kirchoff, ''The slow rotation of a sphere in a viscous fluid,'' in *Hydrodynamics*, edited by H. Lamb (Dover, New York, 1945).

[33] P. Méléard, C. Gerbaud, T. Pott, L. Fernandes-Puente, I. Bivas, M. Mitov, J. Dufourcq, and P. Bothorel, ''Bending elasticities of model membranes: Influences of temperature and sterol content,'' Biophys. J., **72**, 2616 (1997); M. Rossof, *Vesicles* (Marcel Dekker, New York, 1996).